RESEARCH PAPER

PCCP
www.rsc.org/pccp

Low-temperature catalytic destruction of CCl_4, $CHCl_3$ and CH_2Cl_2 over basic oxides

Pieter Van der Avert[a] and Bert M. Weckhuysen*[ab]

[a] *Centrum voor Oppervlaktechemie en Katalyse, Departement Interfasechemie, KULeuven, Kasteelpark Arenberg 23, 3001 Leuven, Belgium*
[b] *Departement Anorganische Chemie en Katalyse, Debye Instituut, Universiteit Utrecht, Sorbonnelaan 16, 3584 CA Utrecht, The Netherlands. E-mail: b.m.weckhuysen@chem.uu.nl*

Received 8th September 2004, Accepted 14th September 2004
First published as an Advance Article on the web 5th October 2004

The catalytic destruction of CCl_4, $CHCl_3$ and CH_2Cl_2 in the presence of steam has been compared over a series of unsupported and alumina-supported lanthanide and alkaline earth oxides. It was found that (1) the destruction rate over basic oxides decreases with decreasing chlorine content of the CHC compound ($CCl_4 > CHCl_3 > CH_2Cl_2$); (2) the catalyst activity is always higher for lanthanide oxides than for alkaline earth oxides; (3) supported basic oxides are more active than their unsupported counterparts and (4) a stable destruction activity of more than 10 days can be maintained as long as an excess of steam is present in the gas stream. The reaction products are also dependent on the type of chlorinated hydrocarbon. CO_2 and HCl are the products for the destruction of CCl_4 and both compounds are formed from the reaction intermediate Cl_2CO. In the case of $CHCl_3$ a mixture of CO and HCl is produced, partially formed *via* the hydrolysis of the reaction intermediate HClCO. Finally, the reaction products for the destruction of CH_2Cl_2 are HCl, CO and H_2; the latter two are formed from H_2CO decomposition. In the case of supported basic oxides significant amounts of CH_3Cl are produced in the catalytic destruction of CH_2Cl_2, which is catalyzed by the partially uncovered Al_2O_3 support phase. *In situ* Raman and infrared spectroscopy were used to monitor the physicochemical changes taking place in the catalytic solid as well in the gas phase above the catalyst material. Based on these findings a plausible reaction mechanism is proposed. Lanthanide oxides and lanthanide oxide chlorides are both active phases in this catalytic process.

Introduction

Recently, our group reported on a new class of catalytic materials active in the decomposition of CCl_4 in the presence of steam.[1–4] This destruction reaction can be written as follows:

$$CCl_4 + 2H_2O \rightarrow CO_2 + 4\ HCl \qquad (1)$$

It was shown that La_2O_3, Pr_2O_3, Nd_2O_3 and CeO_2 are very active in this reaction and a 10 wt% La_2O_3/Al_2O_3 catalyst exhibited a destruction capacity of 0.289 g CCl_4 g^{-1} h^{-1} at 350 °C.[1,2] Table 1 compares the obtained activity with those of some reference materials. Although comparison is not easy because of the different experimental conditions used, the destruction capacity of the 10 wt% La_2O_3/Al_2O_3 catalyst is superior over the existing oxidation catalysts.[1] Based on spectroscopic, catalytic and theoretical investigations it was concluded that the catalytic reaction consists of a destructive adsorption step of CCl_4 on basic oxygen sites followed by a steam dechlorination step of the formed chlorinated catalytic solid.[3,4] The process starts with the splitting of this first Cl atom during destructive adsorption, most probably catalyzed by a Lewis acid site. The CCl_3 intermediate is then stabilized by a basic oxygen site and the formed O–CCl_3 adsorbate further decomposes by donating another Cl atom to the surface and abstracting the bonding oxygen atom. The generated gas-phase Cl_2CO reaction intermediate has been observed experimentally[3] and reacts further with the surface to form CO_2. The following consecutive reactions apply for La_2O_3:

$$\tfrac{3}{2}CCl_4 + La_2O_3 \rightarrow \tfrac{3}{2}CO_2 + 2LaCl_3 \qquad (2)$$

$$2LaCl_3 + 3H_2O \rightarrow La_2O_3 + 6HCl \qquad (3)$$

Depending on the reaction conditions, more specifically the H_2O to CCl_4 molar ratio, the catalytic material was found to transform dynamically from the metal oxide state (La_2O_3) to the metal oxide chloride (LaOCl) or metal trichloride ($LaCl_3$) state due to bulk diffusion of oxygen and chlorine atoms. Both La_2O_3 and LaOCl are active materials in this reaction, whereas $LaCl_3$ is catalytically inactive. It was also found that an excess of steam in the waste stream is crucial for stable catalyst activity.

In this work, we extend our study to the catalytic hydrolysis over basic oxides of two other chlorinated hydrocarbons (CHCs); *i.e.*, $CHCl_3$ and CH_2Cl_2. These reactions can be written as follows:

$$CHCl_3 + H_2O \rightarrow CO + 3HCl \qquad (4)$$

$$CH_2Cl_2 + H_2O \rightarrow CO + H_2 + 2HCl \qquad (5)$$

On the basis of catalytic and spectroscopic data, a plausible reaction mechanism is proposed explaining the different reaction products formed for these two chlorinated hydrocarbons compared to CCl_4. In addition, the catalytic performances of La_2O_3 materials with different surface areas are also studied, revealing the complexity of the catalytic materials under investigation. Finally, the role of alumina as support will be discussed and guidelines to design more active catalytic solids are proposed.

Experimental section

1. Catalyst preparation

The following alkaline earth and lanthanide oxides have been studied: MgO (Aldrich, 99%, 117 m^2 g^{-1}); CaO (Aldrich, 99.9%, 7 m^2 g^{-1}); SrO (Aldrich, 99.9%, 2 m^2 g^{-1}), BaO (Aldrich, 97%, 0.25 m^2 g^{-1}), La_2O_3 (Acros, 99%, 1 m^2 g^{-1}), CeO_2 (Aldrich, 99, 9%, 0.25 m^2 g^{-1}), Pr_2O_3 (Alfa Aesar,

DOI: 10.1039/b413876g

Table 1 Comparison of the destruction capacities of different catalytic solids for the destruction of CCl_4 at 350 °C, together with the experimental conditions[1]

Catalytic system	Loading of CCl_4 (ppm)	GHSV/h^{-1}	Destruction capacity/g CCl_4 h^{-1} g^{-1} catalyst
$LaMnO_3$	500	6000	0.004
$LaCoO_3$	500	6000	0.016
Co–Y	1000	1367	0.009
Cr–Y	1000	1367	0.009
Cr_2O_3/Al_2O_3	1000	15000	0.036
Pt, Pd, or Rh/TiO_2	1000	15000	0.102
La_2O_3	47000	800	0.145
La_2O_3/Al_2O_3	47000	800	0.289

99.9%, 3 m^2 g^{-1}) and Nd_2O_3 (Alfa Aesar, 99.9%, 3 m^2 g^{-1}). Alumina-supported (Condea, surface area of 220 m^2 g^{-1}; pore volume of 0.4 ml g^{-1}, 99% purity and zero point of charge of 8.5) alkaline earth and lanthanide oxide-based catalysts were prepared by incipient wetness impregnation of aqueous metal acetates. The origin and purity of the corresponding metal acetate salts were as follows: Mg (Aldrich, 99%), Ca (Avocado, 98%), Sr (Avocado, 98%), Ba (Aldrich, 99%), La (Fluka, 97%), Ce (Aldrich, 99.9%), Pr (Aldrich, 99.9%) and Nd (Aldrich, 99.9%). After impregnation, samples were dried at 100 °C for 1 h. The impregnation was repeated until the desired metal oxide loading was obtained. The metal loading of the supported catalysts in moles was always equal and corresponds to 10 wt% for lanthanum. In addition, La_2O_3 catalysts with different surface areas have been prepared *via* the sol–gel procedure. For this purpose, $La(NO_3)_3 \cdot 7H_2O$ (Aldrich, 99.9%) was dissolved in water and subsequently NaOH (BDH, > 99%) was added to this solution to initiate gel formation. The pH increased to a value around 7–8 and the obtained gel was kept at room temperature for a fixed time, followed by centrifugation and washing with demineralized water. After successive washing steps to remove NaOH the gel was dried at 100 °C, followed by calcination at 450 °C in O_2 for 7 h. By varying the ripening time and the La concentration, La_2O_3 materials with a different surface area could be obtained. The synthesized La_2O_3 materials possess the following surface area (m^2 g^{-1}): 21, 26, 31, 35, 40, 53, numbers which are significantly higher than the commercially available La_2O_3 material (1 m^2 g^{-1}). All catalysts were granulated and the 0.25–0.50 mm sieve fraction was used for testing and characterization.

2. Activity testing

Activity tests were performed on 1 g of a catalyst in a fixed-bed reactor at atmospheric pressure. Details of the experimental set-up have been published elsewhere.[1,3,4] Samples were pretreated in 0.6 L h^{-1} O_2 flow at 450 °C overnight. During the reaction, a He flow at 0.48 L h^{-1} was passed through a saturator filled with CCl_4 (VEL, pro analyze), $CHCl_3$ (BDH, 99.0–99.8%) or CH_2Cl_2 (BDH, 99.8%) and maintained at 0 °C in an ice-bath in order to preserve a constant vapor pressure, and, consequently, the same CHC concentration. The CCl_4, $CHCl_3$ and CH_2Cl_2 loadings are respectively 0.00098, 48000 ppm), 0.0018 (84700 ppm) and 0.0023 (105000 ppm) mol h^{-1}. The space velocity (GHSV) was 800 h^{-1} and as Table 1 indicates the waste streams under investigation are heavily loaded with CHCs as compared to literature studies. Water was added to the reactor at the rate of 0.0012 L h^{-1} *via* a Metrohm dosimeter and evaporated when in contact with the reactor walls and bed. The H_2O to CHC molar ratio was 61, 28 and 22 for CCl_4, $CHCl_3$ and CH_2Cl_2, respectively, and thus an excess of steam was added to the reaction mixture. It was shown in previous work that an excess of steam in the inlet stream is essential for the stability of the catalyst system.[3] Most of the water in the effluent stream was trapped with an impinger at room temperature. The remaining gases were analyzed with a gas chromatograph (HP 4890D with an FID detector and methanator) using a packed Hayesep Q CP column (80–100 mesh, 3 m). Conversions have been calculated by taking into account the amount of chlorinated hydrocarbon before and after reaction and the corresponding sensitivity factors of the chlorinated hydrocarbon.

3. Catalyst characterization

Surface areas of the materials were determined by N_2 sorption measurements with a Micromeritics ASAP 2400 instrument. Raman spectra were collected with a Holoprobe Kaiser Optical RXN-532 spectrometer equipped with a holographic notch filter, a laser Raman excitation of 532 nm and a CCD camera. A special *in situ* Raman cell was used that could be heated in a stream of reagents at elevated temperatures. Infrared spectra were collected with a Nicolet 730 FT-IR spectrometer. A special *in situ* infrared cell was designed in which a catalyst wafer was placed in a quartz cell equipped with KBr windows. X-ray diffraction (XRD) measurements were performed with a Siemens D5000 diffractometer using a Ni-filtered CuKα source with a wavelength of 0.154 nm. Scanning electron microscopy (SEM) was performed on a Philips XL30FEG instrument. The samples were spread out on a carbon layer. Depending on the conductivity of the samples, a small amount of noble metal was vaporised on the sample to prevent charging. The analysis of the elements was carried out with an energy dispersive spectrometer (EDS) detector from EDAX. Coke formation has been evaluated with thermogravimetric analysis (TGA) using a TGA92 Setaram instrument. The materials were heated up to 800 °C (heating rate of 10 °C min^{-1}) in a He/O_2 stream.

Results and discussion

1. Catalytic activity of unsupported basic oxides

Fig. 1 compares the conversion of CCl_4, $CHCl_3$ and CH_2Cl_2 over the alkaline earth oxides and lanthanide oxides after 7 h of operation at 350 °C. There are two important observations to make: (1) the destruction rate decreases with decreasing chlorine content of the CHC; *i.e.*, in the order: CCl_4 > $CHCl_3$ > CH_2Cl_2. This observation is in line with the expected trend since the Gibbs free energy of this reaction decreases with increasing chlorine content (ΔG is equal to −384.5, −214.2 and −112.3 kJ mol^{-1} for CCl_4, $CHCl_3$ and CH_2Cl_2, respectively). (2) Lanthanide oxide-based catalysts are always more active than alkaline earth oxide-based catalytic systems, regardless of the type of CHC fed to the reactor. The maximum conversion over La_2O_3 is 62% for CCl_4, 37% for $CHCl_3$ and 16% for CH_2Cl_2. This comparison holds also for materials with similar surface area; *i.e.*, when we compare the specific conversion (%) of *e.g.* BaO with that of CeO_2 (both materials have a surface area of 0.25 m^2 g^{-1}) and of *e.g.* SrO with that of Pr_2O_3 (both materials have a surface area of 2–3 m^2 g^{-1}). It is, however, important to indicate that the surface areas of the unsupported basic oxides decrease during reaction, preventing a simple relationship between catalyst activity and catalyst surface area (*vide infra*).

Besides the catalyst activity it is also important to discuss the differences in product formation. Fig. 1B compares the product distribution in the outlet gas stream of La_2O_3 after 7 h of operation at 350 °C. Similar observations were made for the other unsupported alkaline earth metal and lanthanide oxide catalysts. It was found that catalytic destruction of CCl_4 streams results in the formation of CO_2 and only traces of CO. In the catalytic destruction of $CHCl_3$ the main product is,

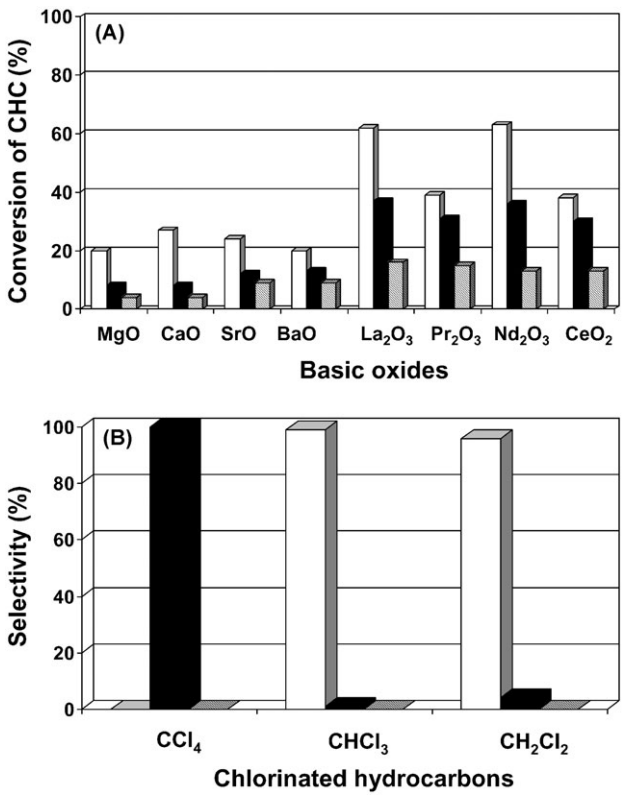

Fig. 1 (A) Conversion of CCl_4 (white bars), $CHCl_3$ (black bars) and CH_2Cl_2 (traced bars) over unsupported alkaline earth metal and lanthanide oxides after 7 h of operation at 350 °C. (B) Selectivity for the conversion of CCl_4, $CHCl_3$ and CH_2Cl_2 over La_2O_3 after 7 h of operation at 350 °C: CO (white bars), CO_2 (black bars) and CH_3Cl (traced bars).

however, CO, which is the expected reaction product based on reaction 4. The amount of CO_2 is always negligible and floats around 1–2%. CH_2Cl_2 destruction over La_2O_3 also results in the formation of CO and small amounts of CO_2 (2–4%). This is in line with reaction 5. A plausible explanation for the formation of CO is the direct decomposition of the expected reaction intermediates CH_2O and CHClO, according to:

$$CH_2O \rightarrow CO + H_2 \quad (6)$$

$$CHClO \rightarrow CO + HCl \quad (7)$$

It can be postulated that the small amounts of CO_2 can be formed by the combination of CO and Cl_2 to Cl_2CO, which is easily hydrolyzed with H_2O at 350 °C to CO_2 and HCl:

$$CO + Cl_2 \rightarrow COCl_2 \quad (8)$$

$$Cl_2CO + H_2O \rightarrow CO_2 + HCl \quad (9)$$

It should, however, be stated that we have never observed any Cl_2 in the exit gas stream during the catalytic destruction of the three CHCs under investigation.

In an attempt to enhance the catalytic performances of unsupported basic oxides we have synthesized a series of La_2O_3 materials ranging in surface area between 1 and 52 m^2 g^{-1}. The results of these materials for the destruction of CH_2Cl_2 are summarized in Table 2. Comparable results have been obtained for the two other CHCs as well. It is evident that there is no clear trend between the initial surface area of La_2O_3 and the conversion activity, although the material with the highest surface area (52 m^2 g^{-1}) is the most active catalyst. On the other hand, the catalyst surface area of La_2O_3 materials is significantly reduced under reaction conditions and in the case of the most active La_2O_3 the surface area is reduced to 22 m^2 g^{-1}. Although this material is not the material with the highest surface any more, it is still the best performing catalyst material. Thus, there is no simple correlation between catalyst activity and surface area; *i.e.*, the number of exposed La-ions at the catalyst surface. Most probably, the synthesis conditions are responsible for the creation of more active sites at the La_2O_3 surface. Currently, we are studying the surface acid–base properties of these different La_2O_3 materials with infrared spectroscopy and probe molecules (CO, CO_2 and pyridine) in order to obtain a better insight into the number of potential active sites and if possible to correlate these active sites with catalytic performances.

Table 2 CH_2Cl_2 conversion (%) in the presence of steam at 350 °C over La_2O_3 catalysts with different surface areas

Surface area before reaction/m^2 g^{-1}	Surface area after reaction/m^2 g^{-1}	Conversion (%) after 7 h on stream
1	1	16
21	14	16
26	12	13
31	13	15
35	18	19
40	30	18
53	22	27

2. Catalytic activity of supported basic oxides

The idea of increasing the surface area of the active La_2O_3 phase can be further explored by spreading La_2O_3 at the surface of a support oxide. It was indeed found that higher conversions were obtained by supporting basic oxides onto Al_2O_3. Other supports such as TiO_2 and SiO_2 also gave good results, but the conversion levels were about 10–15% lower than in the case of alumina-supported basic oxides. We also found that lanthanide acetates were the best salts for impregnating lanthanide ions onto the alumina support and less active catalyst materials were made if nitrate or sulfate was the counteranion. Another important aspect is the stability of the Al_2O_3 support under reaction conditions. First of all, we observed that the surface area of alumina does not significantly decrease during reaction and remains around 200 m^2 g^{-1}. Secondly, XRD indicates that no $AlCl_3$ and/or α-Al_2O_3 phases are formed during catalytic destruction of the different CHCs for prolonged reaction times. As a consequence, alumina seems to be a good support to keep the active phase dispersed at its surface.

The results of the conversion of the different CHCs over alumina-supported alkaline earth metal and lanthanide oxides are shown in Fig. 2A. To make relevant comparisons, the metal loadings of the supported catalysts in moles are equal to that of the best performing catalyst, 10 wt% La on Al_2O_3. It can be concluded that the catalyst activity drastically increased by spreading the active basic oxide compound on a carrier support. In addition, the two main observations described above for unsupported basic oxides are still valid for the supported basic oxide catalysts as well. Our best performing catalyst, 10 wt% La on Al_2O_3, converts at 350 °C 100% of CCl_4, 68% of $CHCl_3$ and 53% of CH_2Cl_2.

In contrast to unsupported basic oxides, alumina-supported basic oxides form besides CO significant amounts of CH_3Cl in the destruction of CH_2Cl_2 (Fig. 2B). The ratio CO : CH_3Cl is around 2 : 1 for a La on Al_2O_3 catalyst, and similar ratios have been observed for other catalytic systems. The formation of CH_3Cl could be explained by the mechanism proposed by Van den Brink *et al.*[5] These authors have studied the oxidation of CH_2Cl_2 over bare Al_2O_3 in the presence of H_2O and observed the formation of CH_3Cl. Their reaction mechanism involves the reaction of CH_2Cl_2 with a surface hydroxyl group of alumina and the formed chloromethoxy species is further converted into a chemisorbed formaldehyde analogue. In a

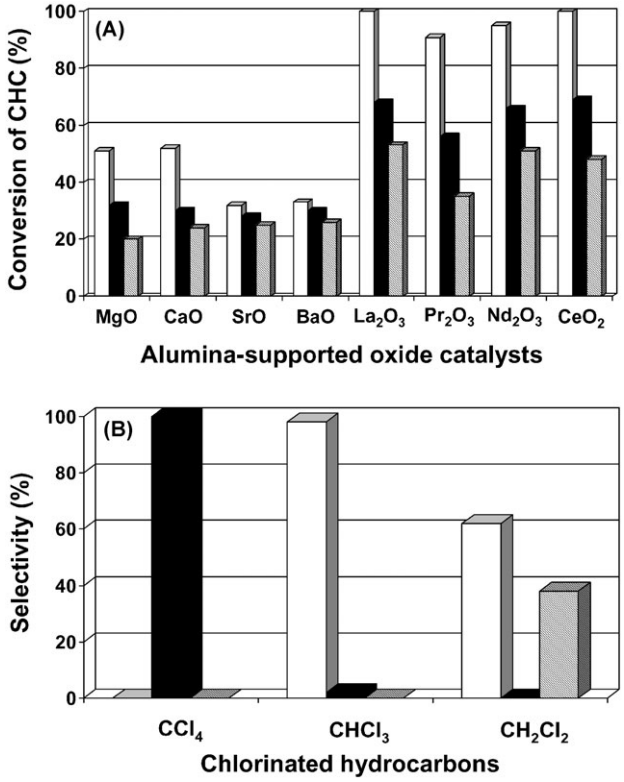

Fig. 2 (A) Conversion of CCl_4 (white bars), $CHCl_3$ (black bars) and CH_2Cl_2 (traced bars) over alumina-supported alkaline earth metal and lanthanide oxides after 7 h of operation at 350 °C. (B) Selectivity for the conversion of CCl_4, $CHCl_3$ and CH_2Cl_2 over La_2O_3/Al_2O_3 after 7 h of operation at 350 °C: CO (white bars), CO_2 (black bars) and CH_3Cl (traced bars).

second step, two chemisorbed formaldehyde molecules will react with HCl and H_2O to form CH_3Cl and CO. This disproportionation reaction, involving a hydride shift, is required to obtain the end products, including the starting material Al_2O_3. Steam converts the formed $AlCl_3$ again to Al_2O_3 and takes part directly in the disproportionation reaction. This hypothesis has been further tested by using our bare Al_2O_3 support as catalyst material and as expected CH_3Cl and CO have been formed out of CH_2Cl_2 under identical catalytic conditions.

This reaction, however, suggests that alumina-supported alkaline earth metal and lanthanide oxide catalysts are not fully dispersed and that free Al_2O_3 patches are present at the catalyst surface. This is indeed the case as illustrated in Fig. 3 by a SEM picture of a La_2O_3/Al_2O_3 catalyst before and after catalyzing the decomposition of CH_2Cl_2 for 7 h at 350 °C. The grey material is the alumina phase covered with only very small amounts of La, whereas the white spots are La-enriched phases. This is evident from the EDAX analysis along the indicated scanning lines. Before reaction the La-rich phases have a size of about 10 μm and are composed of most probably La_2O_3. After reaction La-rich phases of equal or smaller size are observed. In contrast, these phases contain comparable amounts of La and Cl, pointing towards the formation of LaOCl. Here again, alumina is not fully covered by a La-rich phase, although clearly some Cl is covering Al_2O_3. Thus, although lanthanide acetate salts have been used for the preparation of the best performing supported catalysts, patches of lanthanide oxide or lanthanide oxide chloride are still inhomogeneously distributed over the alumina surface in the catalytic solids.

A second disadvantage of the alumina-supported basic oxide catalysts is the formation of some coke at the catalyst surface during reaction as observed with TGA of the catalytic solids after 7 h on stream at 350 °C. The amount of coke is, however,

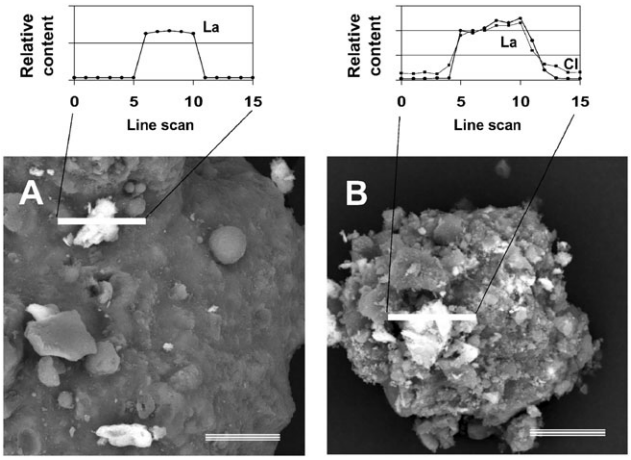

Fig. 3 Scanning electron micrograph of a La_2O_3/Al_2O_3 catalyst before reaction (A) and after 7 h on stream in the destruction of CH_2Cl_2 at 350 °C (B), together with the relative amount of La and Cl as determined with EDAX along the indicated analysis line. The bottom right line has a length of 10 μm.

always low (0–3 wt% coke) and its amount increases with decreasing chlorine content of the CHC and is higher for alumina-supported lanthanide and alkaline earth metal oxide than for their unsupported counterparts. For example, coke formation equals 0.0004 mol h^{-1} for La_2O_3/Al_2O_3 and 0.00004 mol h^{-1} for La_2O_3 for the destruction of CH_2Cl_2 at 350 °C, implying that the acidity of the alumina support takes part in the coke formation. Another check for coke formation is the gaseous carbon balance over supported catalysts. This balance is 100% for CCl_4, and floats between 95 and 100% for the two other CHCs, fairly in line with the TGA results.

Finally, it is important to recall that the results presented in Figs. 1 and 2 only hold for a reaction temperature of 350 °C. It is obvious that the conversion increases with increasing reaction temperature and reaches 100% over a La_2O_3/Al_2O_3 catalyst for CCl_4, $CHCl_3$ and CH_2Cl_2 at reaction temperatures of 350, 400 and 450 °C, respectively. This is in line with the C–H and C–Cl bond strengths (E_b = 411 *vs.* 327 kJ mol^{-1}). Another important reaction parameter is the presence of steam. In line with our previous experiments for the catalytic destruction of CCl_4,[3] we observed for the destruction of $CHCl_3$ and CH_2Cl_2 a positive influence of the presence of steam both on activity and catalyst stability. Indeed, switching off the steam results in an instant drop in catalyst activity, while deactivated catalysts can regain their activity by switching on the steam (Fig. 4). Thus, steam is essential for the performance of the catalytic solids. If steam is present in sufficient amounts; *i.e.*, $[H_2O]:[CHC] \geq 20$, a stable activity could be maintained for more than 10 days. This is illustrated in Fig. 5.

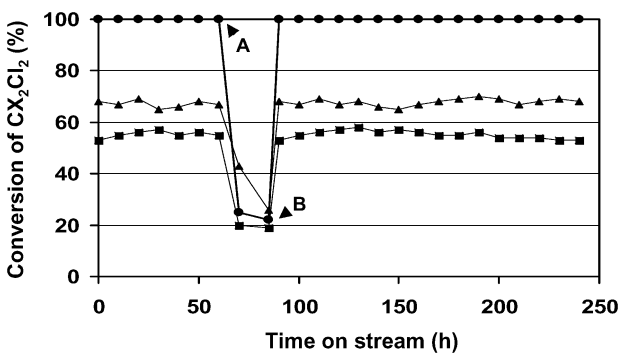

Fig. 4 Effect of steam on the catalytic activity of a La_2O_3/Al_2O_3 catalyst at 350 °C for the destruction of CCl_4 (●), $CHCl_3$ (▲) and CH_2Cl_2 (■): (A) switching off the steam and (B) switching on the steam again.

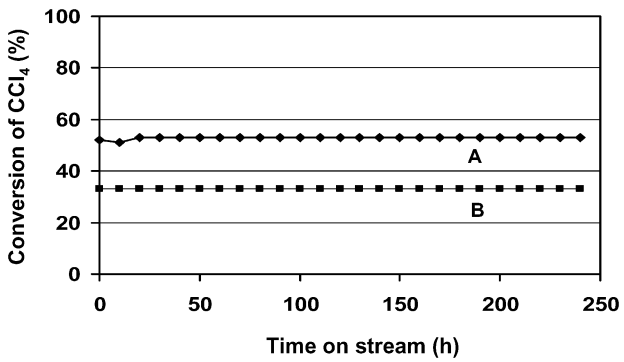

Fig. 5 CCl_4 conversion in the presence of steam at 300 °C as a function of time on steam over La_2O_3/Al_2O_3 (A) and La_2O_3 (B) catalysts over an extended time period.

3. *In situ* spectroscopic characterization

In situ Raman spectra collected during CCl_4, $CHCl_3$ and CH_2Cl_2 decomposition in the presence of steam (reactions 1, 4 and 5) over La_2O_3 after 7 h of reaction are shown in Fig. 6 and compared with those of La_2O_3, LaOCl and $LaCl_3$ reference compounds. The spectra indicate that La_2O_3 is the main catalytic phase present in the reactor in the presence of CCl_4, whereas LaOCl is formed in the presence of either $CHCl_3$ or CH_2Cl_2. In any case, no significant amounts of $LaCl_3$ could be detected after 7 h on stream. The presence of LaOCl in the case of $CHCl_3$ and CH_2Cl_2—containing less chlorine atoms per molecule than CCl_4—can be explained by the higher loadings of both CHCs in the feed. On the other hand, longer reaction times (*e.g.* 36 h) lead to the formation of both LaOCl and $LaCl_3$ (Table 3). Finally, it is important to notice that the 375 cm^{-1} Raman peak has been assigned previously to a luminescence effect.[3]

Similar *in situ* Raman spectra have been obtained for CeO_2, Pr_2O_3 and Nd_2O_3 after 7 and 36 h on stream. Table 3 summarizes the Raman shifts of some reference materials as well as the Raman shifts of the catalytic solids after 7 and 36 h on stream. As discussed above, in the case of CCl_4 after 7 h on stream CeO_2, Pr_2O_3 and Nd_2O_3 are the main phases, whereas CeOCl, PrOCl and NdOCl are the dominant phases in a catalyst destroying $CHCl_3$ or CH_2Cl_2 for 7 h. Thus, the family

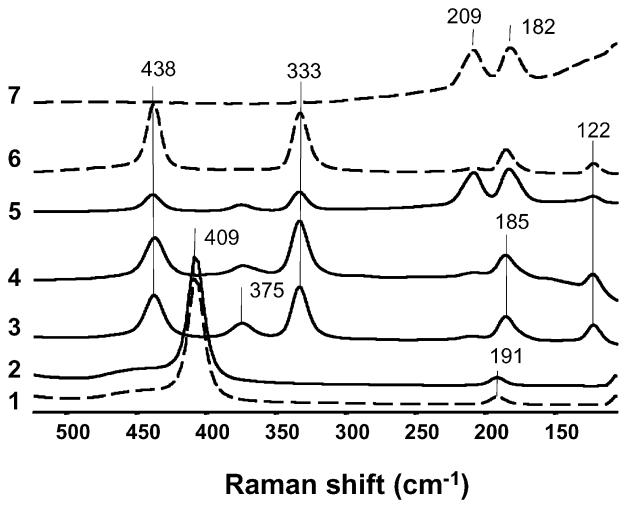

Fig. 6 *In situ* Raman spectra collected during CCl_4, $CHCl_3$ and CH_2Cl_2 decomposition in the presence of steam over La_2O_3 after 7 h of reaction at 350 °C: (1) La_2O_3 dehydrated in N_2 at 550 °C; (2) La_2O_3 after reaction with CCl_4; (3) La_2O_3 after reaction with $CHCl_3$; (4) La_2O_3 after reaction with CH_2Cl_2; (5) La_2O_3 after reaction with CH_2Cl_2; this material is the one collected from the reactor in point B of Fig. 5; (6) LaOCl dehydrated in N_2 at 800 °C; and (7) $LaCl_3$ dehydrated in N_2 at 550 °C.

Table 3 Raman shifts of Ln_2O_3, LnOCl and $LnCl_3$ reference compounds, together with those of the catalytic solids treated with CCl_4, $CHCl_3$ and CH_2Cl_2 at 350 °C for 7 and 36 h

Element	Solid	Raman shift/cm^{-1}	Ref.
La	La_2O_3	107, 195, 410	7, 8
	LaOCl	125, 188, 215, 335, 440	7, 9, 10
	$LaCl_3$	108, 180, 211	7, 11, 12
	La_2O_3 treated with CCl_4 for 7 h	106, 191, 409	This work
	La_2O_3 treated with CCl_4 for 36 h	125, 188, 215, 335, 440; 108, 180, 211	This work
	La_2O_3 treated with $CHCl_3$ for 7 h	122; 185, 209, 333, 438	This work
	La_2O_3 treated with $CHCl_3$ for 36 h	125, 188, 215, 335, 440; 108, 180, 211	This work
	La_2O_3 treated with CH_2Cl_2 for 7 h	121, 185, 209, 332, 439	This work
	La_2O_3 treated with CH_2Cl_2 for 36 h	125, 188, 215, 335, 440; 108, 180, 211	This work
Ce	CeO_2	102, 250, 454	7
	CeOCl	125, 188, 217, 321, 469	7
	$CeCl_3$	108, 183, 217	7
	CeO_2 treated with CCl_4 for 7 h	100, 246, 450	This work
	CeO_2 treated with CCl_4 for 36 h	125, 188, 217, 321, 469; 108, 183, 217	This work
	CeO_2 treated with $CHCl_3$ for 7 h	122, 186, 213, 319, 467	This work
	CeO_2 treated with $CHCl_3$ for 36 h	125, 188, 217, 321, 469; 108, 183, 217	This work
	CeO_2 treated with CH_2Cl_2 for 7 h	122, 185, 214, 318, 466	This work
	CeO_2 treated with CH_2Cl_2 for 36 h	125, 188, 217, 321, 469; 108, 183, 217	This work
Pr	Pr_2O_3	105, 192, 415	13
	PrOCl	121, 185, 216, 346, 458	9
	$PrCl_3$	108, 186, 216	14
	Pr_2O_3 treated with CCl_4 for 7 h	102, 190, 412	This work
	Pr_2O_3 treated with CCl_4 for 36 h	120, 186, 216, 345, 457; 108, 187, 216	This work
	Pr_2O_3 treated with $CHCl_3$ for 7 h	119, 182, 213, 344, 456	This work
	Pr_2O_3 treated with $CHCl_3$ for 36 h	121, 186, 217, 346, 458; 109, 187, 217	This work
	Pr_2O_3 treated with CH_2Cl_2 for 7 h	118, 181, 212, 343, 455	This work
	Pr_2O_3 treated with CH_2Cl_2 for 36 h	120, 185, 217, 346, 457; 108, 186, 215	This work
Nd	Nd_2O_3	102, 190, 434	9
	NdOCl	121, 184, 220, 353, 465	9
	$NdCl_3$	104, 184, 219	15
	Nd_2O_3 treated with CCl_4 for 7 h	100, 186, 431	This work
	Nd_2O_3 treated with CCl_4 for 36 h	121, 185, 221, 353, 467; 105, 185, 219	This work
	Nd_2O_3 treated with $CHCl_3$ for 7 h	119, 180, 218, 350, 462	This work
	Nd_2O_3 treated with $CHCl_3$ for 36 h	121, 184, 220, 354, 466; 105, 184, 219	This work
	Nd_2O_3 treated with CH_2Cl_2 for 7 h	119, 180, 218, 350, 462	This work
	Nd_2O_3 treated with CH_2Cl_2 for 36 h	121, 184, 221, 353, 466; 105, 184, 220	This work

of the lanthanide oxides (Ln_2O_3) gradually transforms during reaction into the corresponding lanthanide oxide chloride

Table 4 Catalytic activity (conversion in %) of bulk La_2O_3, LaOCl and $LaCl_3$ for CCl_4, $CHCl_3$ and CH_2Cl_2 destruction after 7 h on stream in the presence of steam at 350 °C. The reported activity of $LaCl_3$ materials should be considered with care since hydrated $LaCl_3$ easily transforms during heating in the reactor into LaOCl so the activity of $LaCl_3$ could be partially due to the presence of LaOCl instead of $LaCl_3$

Compound	CCl_4	$CHCl_3$	CH_2Cl_2
La_2O_3	62	34	15
LaOCl	60	26	14
$LaCl_3$	5	24	11

(LnOCl) and after prolonged reaction times (*i.e.*, 36 h) partially to lanthanide chloride ($LnCl_3$). This change is also associated with a decrease in surface area. This observation confirms the earlier reported dynamics of the catalyst systems under investigation.[3] The almost complete transformation of Ln_2O_3 into LnOCl takes place according to:

$$Ln_2O_3 + \tfrac{1}{2}\,CCl_4 \rightarrow 2LnOCl + \tfrac{1}{2}CO_2 \qquad (10)$$

This implies that LnOCl, in addition to Ln_2O_3, is an active phase. This hypothesis has been evaluated by testing the activity of bulk LaOCl in the destruction of CH_2Cl_2 and $CHCl_3$. As expected, similar activities were obtained as in the case of La_2O_3 (Table 4). Continuing the reaction for extended time periods or shutting down the steam supply results in the (partial) transformation of the catalyst material to $LaCl_3$ (Table 3). These processes can be written as follows:

$$2LaOCl + CCl_4 \rightarrow 2LaCl_3 + CO_2 \qquad (11)$$

At this stage the catalyst material becomes less active and separate catalytic experiments on $LaCl_3$ for the destruction of CH_2Cl_2 and $CHCl_3$ show that the initial activity of $LaCl_3$ is indeed smaller than those of LaOCl and La_2O_3 (Table 4). However, whereas in the case of CCl_4, $LaCl_3$ seems to be almost completely inactive, this is certainly not the case for $CHCl_3$ and CH_2Cl_2. One explanation could be that $LaCl_3$ is

Table 5 FT-IR absorption bands of the gas phase molecules detected in the presence of a La_2O_3 catalyst at 350 °C

Chlorinated hydrocarbon	Absorption bands/cm^{-1}	Assignments based on ref. 16
CCl_4	2363, 2340 (most intense)	C=O stretch of CO_2
	2175, 2112	C=O stretch of CO
	3550–3200, 1628	O–H stretch and H–O–H bending of H_2O
	1820, 1831	C=O stretch of $COCl_2$
$CHCl_3$	3033, 2967	C–H stretch
	2408, 2398	C–Cl overtone stretch
	2363, 2340	C=O stretch of CO_2
	2175, 2112 (most intense)	C=O stretch of CO
	3550–3200, 1628	O–H stretch and H–O–H bending of H_2O
	1542, 1442	C–Cl overtone stretch
	1218, 1201	C–Cl stretch
CH_2Cl_2	3001, 2995	C–H stretch
	2695, 2686	C–Cl overtone stretch
	2363, 2340	C=O stretch of CO_2
	2175, 2112 (most intense)	C=O stretch of CO
	1464, 1455	C–Cl overtone stretch
	3550–3200, 1628	O–H stretch and H–O–H bending of H_2O
	1280, 1261	C–Cl stretch

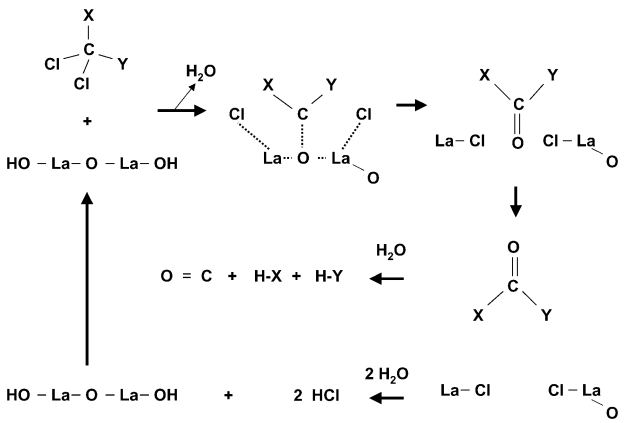

Fig. 7 Reaction scheme for the destruction of CCl_2XY (with X = H and Y = Cl for $CHCl_3$ and X = Y = H for CH_2Cl_2) over La_2O_3 in the presence of steam.

partially transformed into LaOCl during heating in the reactor. Further studies should clarify these observations. Finally, we recall that these bulk transformation phenomena as observed with *in situ* Raman spectroscopy could not be detected for the alumina-supported lanthanide oxide catalysts because of strong laser fluorescence.[3]

In situ infrared spectra of the gas phase have been collected to investigate the formation of possible gaseous reaction intermediates. Table 5 summarizes the FT-IR absorption bands of the gas phase molecules detected during reaction over La_2O_3 and La_2O_3/Al_2O_3 at 350 °C in the presence of steam and CCl_4, $CHCl_3$ or CH_2Cl_2, together with their assignments. Unlike in the case of CCl_4 where $COCl_2$ could clearly be identified as a reaction intermediate,[3] no other gaseous molecules other than those found by gas chromatography in the gas outlet (*e.g.* CO and CO_2) were detected. Since we anticipate that the same reaction mechanism is applicable as previously proposed for the destruction of CCl_4 over La_2O_3, CH_2O and CHClO are the expected reaction intermediates for the destruction of CH_2Cl_2 and $CHCl_3$, respectively. Their absence in the infrared gas phase spectra could be explained by their low stability under the applied reaction conditions. Both reaction intermediates will be readily hydrolysed in the presence of steam resulting in the formation of CO and H_2/HCl according to reactions 6 and 7. We indeed observed high amounts of CO in the *in situ* FTIR cell for the catalytic destruction of CH_2Cl_2 and $CHCl_3$ (Table 5). Other evidence for the catalytic decomposition of HClCO comes from the work of Jasien.[6] This author performed theoretical calculations on the $AlCl_3$-catalyzed decomposition of HClCO. It was found that the presence of $AlCl_3$ resulted in a large decrease of the activation energy for the decomposition reaction of HClCO.

A plausible reaction scheme summarizing the current experimental observations is given in Fig. 7. The catalytic destruction occurs *via* an initial adsorption step of the chlorinated hydrocarbon on the basic oxide surface, in which the chlorine atoms are attached to the catalyst surface, followed by a dechlorination step of the formed chlorinated solid by steam and the formation of hydrochloric acid. CO is proposed to be formed from the reaction intermediate HClCO (for $CHCl_3$) or H_2CO (for CH_2Cl_2), whereas CO_2 is proposed to be formed from the reaction intermediate Cl_2CO (for CCl_4).

Conclusions

The following conclusions can be drawn from this work:

(1) Basic oxides are very active materials for the destruction of CCl_4, $CHCl_3$ and CH_2Cl_2 in the presence of steam between 200 and 450 °C. The ease of catalytic destruction decreases with decreasing chlorine content of the chlorinated

hydrocarbon and is the highest for alumina-supported lanthanide oxides. Stable destruction activities are achieved as long as excess steam is added to the gas stream.

(2) The catalytic hydrolysis of CCl_4 leads to the formation of CO_2 and HCl, whereas the catalytic destruction of $CHCl_3$ and CH_2Cl_2 results in respectively a mixture of CO and HCl and a mixture of H_2, CO and HCl. CO and HCl are proposed to be formed directly from HClCO (for $CHCl_3$), H_2CO decomposition results in the formation of CO, HCl and H_2 (for CH_2Cl_2), whereas CO_2 and HCl are formed from Cl_2CO (for CCl_4). Alumina-supported lanthanide oxides also produce significant amounts of CH_3Cl, which is associated with the catalytic performance of the partially uncovered alumina support phase. Another disadvantage of the alumina support is the enhanced formation of coke. Future work clearly should be directed towards the use of other and most probably non-oxidic catalyst supports, such as carbon nanofibers.

(3) Catalytic destruction of CCl_4, $CHCl_3$ and CH_2Cl_2 with lanthanide oxides is assumed to proceed over a basic surface oxygen site. The active phases La_2O_3 and LaOCl contain these basic surface oxygen sites and their relative concentration is related to the preparation method of the La_2O_3 material. Future infrared work with probe molecules should unravel structural differences between catalytically different LaOCl and La_2O_3 materials with increasing surface areas.

Acknowledgements

This work was supported by the Instituut voor Aanmoediging van Innovatie door Wetenschap en Technologie in Vlaanderen (IWT-Vlaanderen; project ADV/990177). The authors acknowledge fruitful discussions with R. Schoonheydt (KULeuven), G. Mestl (Nanoscape), I. Langhans (CQ), K. Ooms (CQ), D. van Deynse (Tessenderlo Chemie), Y. Sergeant (Tessenderlo Chemie), M. Belmans (Tessenderlo Chemie) and T. Visser (Utrecht University). The authors also thank H. De Winne (KULeuven) for catalytic testing, O. Manoilova (Utrecht University) for the Raman experiments and M. Versluijs-Helder (Utrecht University) for SEM measurements. B.M.W. acknowledges the Dutch Science Foundation (NWO-CW) for a Van der Leeuw and VICI grant.

References

1 P. Van der Avert and B. M. Weckhuysen, *Angew. Chem., Int. Ed.*, 2002, **41**, 4730 and references therein.
2 B. Weckhuysen, R. Schoonheydt and P. Van der Avert, *WO 03057318 A1 patent application.*
3 P. Van der Avert, S. G. Podkolzin, O. Manoilova, H. de Winne and B. M. Weckhuysen, *Chem. Eur. J.*, 2004, **10**, 1637.
4 P. Van der Avert, PhD Thesis, Leuven University, 2003.
5 R. W. Van den Brink, P. Mulder, R. Louw, G. Sinquin, C. Petit and J. P. Hindermann, *J. Catal.*, 1998, **180**, 153.
6 P. G. Jasien, *J. Phys. Chem.*, 1994, **98**, 2859.
7 B. M. Weckhuysen, M. P. Rosynek and J. H. Lunsford, *Phys. Chem. Chem. Phys.*, 1999, **1**, 3157.
8 C. R. Gopinath and I. D. Brown, *J. Raman Spectrosc.*, 1982, **12**, 278.
9 Y. Hase, L. Dunstan and M. L. A. Temperini, *Spectrochim. Acta*, 1981, **8**, 597.
10 H. Haeuseler, *J. Raman Spectrosc.*, 1984, **15**, 120.
11 J. Murphy, H. H. Caspers and R. A. Buchanan, *J. Chem. Phys.*, 1964, **40**, 743.
12 S. K. Asawa, R. A. Satten and O. M. Stafsudd, *Phys. Rev.*, 1968, **168**, 987.
13 J. Gouteron, D. Michel, A. M. Lejus and J. Zarembowitch, *J. Solid State Chem.*, 1981, **38**, 288.
14 T. C. Damen, A. Kiel, S. P. S. Porto and S. Singh, *Solid State Commun.*, 1968, **6**, 671.
15 G. Schaack and J. A. Koningstein, *J. Phys. Chem. Solids*, 1970, **31**, 2417.
16 K. Nakamoto, *Infrared and Raman Spectra of Inorganic and Coordination Compounds Part A: Theory and Applications in Inorganic Chemistry*, John Wiley & Sons, Inc., New York, 1997.

